Journal of Solid State Chemistry **153,** 287–293 (2000)
doi:10.1006/jssc.2000.8764, available online at http://www.idealibrary.com on IDEAL®

Ionic Conductivity of Na_2SO_4–Al_2O_3 Composite Electrolytes: Mechanism and the Role of the Preparatory Parameters

Ashish Jain, Sandeep Saha, Prakash Gopalan,[1] and Ajit Kulkarni

Department of Metallurgical Engineering and Materials Science, Indian Institute of Technology, Bombay 400076, India

Received June 30, 1999; in revised form April 17, 2000; accepted May 11, 2000; published online July 7, 2000

A moderate increase in the electrical conductivity of sodium sulfate has been obtained by dispersing alumina particles. The largest enhancement in conductivity for furnace-cooled samples is observed for 5.5 and 35 m/o α-Al_2O_3 compositions. For 35 m/o composition, the conductivity increases by more than 1 order of magnitude at 400°C and 2 orders of magnitude at 200°C. In contrast to the understanding based on many composite electrolyte theories, 0.004 μm alumina brings about the same or even lower enhancement in conductivity as 0.5 μm alumina. Furthermore, contrary to expectations, negligible enhancement is observed when γ-Al_2O_3 is employed. The maximum enhancement in this study is observed for the 4 m/o Al_2O_3 quenched sample: the conductivity increases by 2 orders for the high-temperature phase and by more than 3 orders for the low-temperature phase. © 2000 Academic Press

Key Words: **ionic conductivity; composite electrolytes; role of preparatory parameters; conductivity mechanism in Na_2SO_4–Al_2O_3 systems.**

1. INTRODUCTION

Na_2SO_4 undergoes a transition from low-temperature orthorhombic phase III to highly conducting high-temperature hexagonal phase I at 241°C. The electrical conductivity of Na_2SO_4, explained on the basis of a percolation-type ion-transport mechanism, is relatively low ($\sigma \sim 1.31 \times 10^{-5}$ ohm^{-1} cm^{-1} at 400°C) for practical applications. In the past, several workers have tried to enhance the conductivity of phase I and stabilize it at room temperature by cationic and anionic substitutions (1–4). So far, the largest enhancements, by more than 3 orders of magnitude, have been observed in Sm^{3+}-, La^{3+}-, and Zn^{2+}-doped systems with complete stabilization of phase I at room temperature (4–6). In the Sm^{3+}-doped system, Shahi and Prakash (7) reported $\sigma \approx 5.5 \times 10^{-3}$ ohm^{-1} cm^{-1} at 400°C. A conductivity of $\sim 10^{-1}$ ohm^{-1} cm^{-1} at 300°C would make a Na_2SO_4- based system a potential electrolyte candidate for solid-state batteries, SO_2/SO_3 sensors, etc.

In this work, we have attempted to enhance the conductivity through composite formation. The ionic conductivity of several solid electrolytes has been increased significantly, from 1 to 3 orders of magnitude, by dispersing fine, insulating particles of a second phase (8–10). These dispersoids tend to enhance the defect concentration in the parent lattice through either interface mechanisms or matrix phenomena (11). Maier has contributed significantly to explain the origin of conductivity enhancement in composite electrolyte systems (12–18).

Of the nearly twenty composite systems researched to date, the most well-studied system is LiI where the conductivity increases by 3 orders of magnitude when dispersed with 40 m/o Al_2O_3 (19). Similarly, the ionic conductivity of the low-temperature phase of Li_2SO_4 increases by 3 orders of magnitude when dispersed with 47% Al_2O_3 (20). For Na_2SO_4, however, no prior studies have been undertaken, despite the higher conductivity it exhibits over the other sulfates in the 250–500°C range.

In the present work, we have aimed at enhancing the conductivity of Na_2SO_4 by studying the influence of composition, particle size and form of alumina, and preparatory parameters. An attempt has been made to identify the conductivity enhancement mechanisms operating in this system. We have also tried to correlate our data with a number of existing models for composite electrolytes. The composites have been characterized using X-ray diffraction, differential scanning calorimetry, and impedance spectroscopy techniques.

2. EXPERIMENTAL PROCEDURES

The starting materials were procured from Loba Chemie, India, Aldrich Chemicals, U.S.A., and Condea Chemie, Germany. High-purity Na_2SO_4 (99.99%) was used for measurements made on pure sodium sulfate. Na_2SO_4 of purity in excess of 99.5% was used for preparation of all the composites. Al_2O_3 was prepared from a sol using Disperal

[1] To whom correspondence may be addressed. E-mail: pgopalan@met.iitb.ernet.in.

0022-4596/00 $35.00

Sol P3. Subsequently, finely sized Al_2O_3 (40 Å) was prepared by reacting ultraclean Al pieces with 0.1 N mercuric chloride, dissolving them in water, precipitating the particles in a solution of 2-ethylhexanol and Span 80, and then drying them under infrared. The particles obtained were characterized by surface area measurement techniques and TEM.

Sodium sulfate and alumina were mixed in appropriate mole percentages and stirred thoroughly in deionized water. The mixtures were then heated to a temperature of 1000°C (α-Al_2O_3) or 600°C (γ-Al_2O_3) for 24 h to achieve a fine dispersion of the second-phase particles. The samples were furnace-cooled, ground into fine powders, and pelletized at pressures of around 5 tons/cm^2. The resulting pellets were 2–4 mm thick and around 12 mm in diameter. These pellets were sintered at 600°C for 8 h. They were then gold-coated to provide good contact with the Pt electrodes for the impedance measurements. Identical heat-treatment schedules were followed for all the composites studied.

The DSC measurements were made with a DuPont 9900 calorimeter using a heating rate of 10°C/min. The XRD patterns were recorded with a PW1820 Philips diffractometer using CuK_α radiation. The impedance measurements were carried out as a function of temperature using a computer-controlled Solarotron impedance gain/phase analyzer, Model Schlumberger SI 1260. The measurements were made in the cooling cycle in the frequency range 1 Hz to 32 MHz with a signal amplitude of 100 mV.

3. RESULTS AND DISCUSSION

3.1. DSC

In the absence of high-temperature XRD data and phase diagrams for the $Na_2SO_4(Al_2O_3)$ system, it has been cumbersome to interpret the DSC results. In the 4.75 and 5.5 m/o compositions, peaks in DSC were observed at 201 and 211°C, respectively. A steep rise in conductivity, shown in Fig. 1 and discussed later, was observed at the same temperatures for these compositions. These peaks most likely represent the (III) → (I) phase transition in Na_2SO_4. Similarly, for the 35 m/o composition, the (III) → (I) transition occurs at 203°C, which corresponds to a transition in the conductivity data (Fig. 2) at the same temperature. For some of the compositions, a peak was observed below 110°C, corresponding to the loss of absorbed moisture. Except for the 4.75 m/o Al_2O_3 composition, a peak between 240 and 250°C was observed for all the systems. These could correspond to the appearance or disappearance of an intermediate second phase.

3.2. XRD

At room temperature, Na_2SO_4 appeared to be the majority phase in all the samples. The high-temperature phase

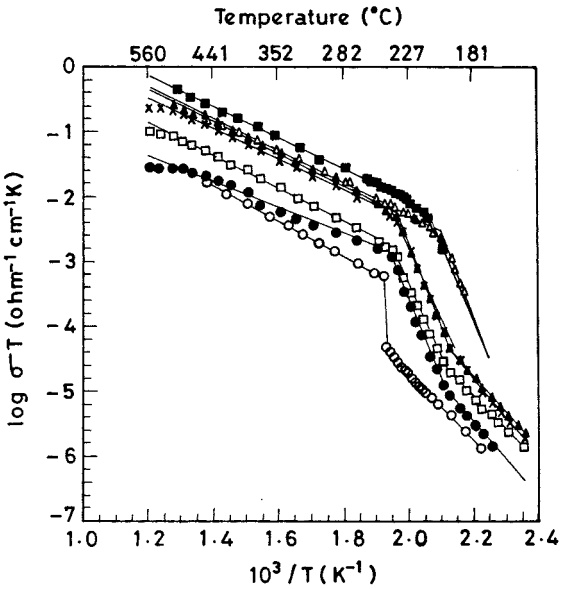

FIG. 1. Log σT vs $10^3/T$ for x m/o α-Al_2O_3 (0.5 μm) compositions: pure Na_2SO_4 (○); $x = 1$ (□), 4 (●), 4.75 (△), 5.5 (■), 7 (▲), 10 (×).

Na_2SO_4(I) was not observed in any of these samples. In compositions of less than 7 m/o, the alumina (α, γ, or θ) phase could not be observed. For most other compositions, α-Al_2O_3 was the predominant phase when the treatment temperature was 1000°C, while γ-Al_2O_3 was observed for samples treated at 600°C. There was apparently no reaction observed between liquid Na_2SO_4 and the dispersed Al_2O_3 even at temperatures around 1000°C. Besides Na_2SO_4 and

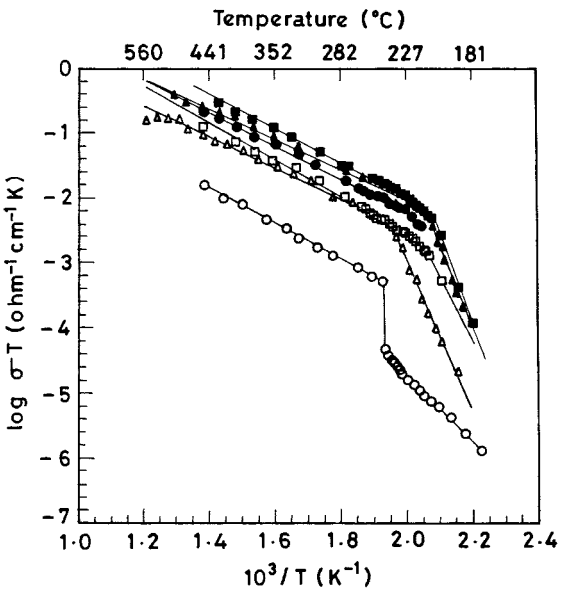

FIG. 2. Log σT vs $10^3/T$ for x m/o α-Al_2O_3 (0.5 μm) compositions: pure Na_2SO_4 (○); $x = 20$ (□), 30 (△), 35 (■), 40 (▲), 50 (●).

Al_2O_3, no third phase could be observed in any of the compositions.

3.3. Conductivity versus Temperature

The log σT versus $10^3/T$ plots for Na_2SO_4–x m/o Al_2O_3 ($x = 0$, 1, 4.75, 5.5, 7, 10, 20, 30, 35, 40, 50) in the cooling cycle are shown in Figs. 1 and 2. For the Na_2SO_4(I) phase ($T_c - 550°C$), the plot indicates a classical Arrhenius-type dependence. No visible trend is observed for variation of either the activation energy or the pre-exponential factor with alumina composition in this temperature range. Table 1 provides relevant data for some of the compositions studied in this work. In a percolation model discussed in the next section, Roman *et al.* (21) have predicted a dependence of the activation energy on the concentration p of the insulating phase as given by

$$E_C = [1 - \varphi(p, \tau)]E_B + \varphi(p, \tau)E_A, \qquad [1]$$

where E_C, E_B, and E_A are the activation energy of the composite, bulk, and interface, respectively. Further, φ is a function of p and τ, a model parameter, given by $\tau^{\varphi} = \sum_{max}/\sum_{o}$. According to this model, the activation energy of the composite sample drops sharply above a threshold concentration p_c'. However, no such trend is observed in the activation energy versus composition behavior.

The maximum enhancement in conductivity was observed for 5.5 and 35 m/o Al_2O_3 compositions. For 5.5 m/o Al_2O_3, the conductivity increased by a factor of 17 at 400°C ($\sigma = 2.2 \times 10^{-4}$ ohm^{-1} cm^{-1} at 400°C) and 260 times at 200°C ($\sigma = 3.3 \times 10^{-6}$ ohm^{-1} cm^{-1}). For 35 m/o composition, the enhancement in conductivity was almost similar. The conductivity increased 23 times ($\sigma = 3.16 \times 10^{-4}$ ohm^{-1} cm^{-1}) at 400°C and 450 times ($\sigma = 5.6 \times 10^{-6}$ ohm^{-1} cm^{-1}) at 200°C. This enhancement was almost comparable with the $Li_2SO_4(Al_2O_3)$ system where the conductivity increased by 3 orders of magnitude. However, this enhancement was less than that observed in Na_2SO_4-based solid solutions with cationic and anionic substitutions. The high-temperature phase was stabilized to 201°C in the 4.75 m/o Al_2O_3 composition, as confirmed by the DSC data.

3.4. Conductivity versus Composition

The conductivity versus composition behavior of most of the reported composite systems has been invariably the same (10, 19). On adding the second-phase particles, the ionic conductivity initially increases, due to the formation of regions with locally enhanced conductivity, until it reaches a maximum. The ionic conductivity then decreases with increasing second-phase content due to the insulating nature of second-phase particles. The peak is observed either around 10 m/o composition (CuCl–Al_2O_3) or 40 m/o composition (LiI–Al_2O_3, Li_2SO_4–Al_2O_3) of the dispersed phase.

However, a different form of conductivity versus composition behavior is observed in the Na_2SO_4–Al_2O_3 system as shown in Fig. 3. Upon addition of alumina, initially there is a sluggish increase in conductivity followed by a sharp, abrupt peak at 5.5 m/o composition. With further addition of alumina, the conductivity decreases and reaches a nearly constant value. However, after 30 m/o Al_2O_3, the conductivity again increases to reach another maxima at 35 m/o Al_2O_3 followed by a subsequent drop. This behavior stands in contrast to that of all other composite systems studied so far.

All the conductivity enhancement mechanisms (9) for composite electrolytes suggested in the literature offer an explanation for the presence of only one peak in the conductivity versus composition plot and, therefore, fail for Na_2SO_4–Al_2O_3 system. It seems then, as pointed out by Dudney (11), that the enhancement in conductivity cannot be attributed to any single mechanism since many mechanisms may operate concomitantly. The sluggish increase in conductivity on adding alumina and the sharp peak at 5.5 m/o are representative of the percolation mechanism suggested by Roman *et al.* (21). On the other hand, the peak

TABLE 1

Composition (m/o Al_2O_3)	σ/σ_{pure} At 200°C	σ/σ_{pure} At 400°C	T_c (°C)	E_a (eV) ($T_c - 550°C$)	σ_0 (ohm^{-1} cm^{-1} K)
0	1	1	241	0.49	5.33
1	5	3	234	0.50	4.99
5.5	263	17	210	0.47	6.33
10	45	8	232	0.46	5.33
20	91	8	215	0.56	7.22
30	10	6	240	0.47	5.23
35	457	23	205	0.52	7.66
40	275	18	215	0.45	5.97
50	—	12	215	0.50	6.64

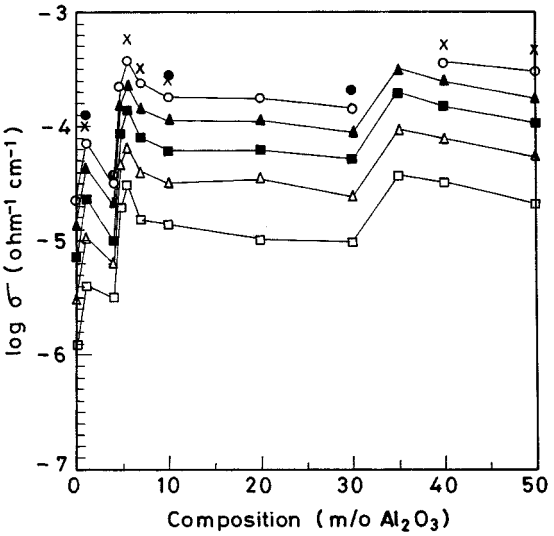

FIG. 3. Log σ vs composition isotherms for 1–50 m/o α-Al_2O_3: (□) 250°C; (△) 300°C; (■) 350°C; (▲) 400°C; (○) 450°C; (×) 500°C; (●) 550°C.

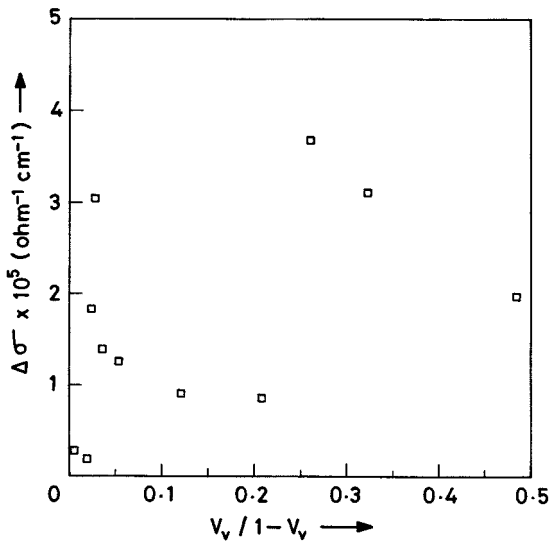

FIG. 4. Variation of $\Delta\sigma$ with alumina volume fraction. Note that the Jow–Wagner model predicts linear behavior.

at 35 m/o Al_2O_3 is characteristic of the dispersoid-induced changes in bulk conductivity, suggested by Wagner (22).

To unambiguously establish the mechanisms operating in this system, we have attempted to correlate our results with the existing conductivity enhancement models for composite electrolyte systems. Most of these models (10, 21, 22) explain the conductivity enhancement behavior in a system assuming that only one mechanism is operative, which again differs from model to model. The most widely studied conductivity enhancement mechanisms (21, 22) are locally enhanced regions of conductivity around the dispersed phase (percolation mechanism) and dispersoid-induced changes in the conductivity of the host material (bulk mechanism). All of these models, therefore, explain the presence of only one peak in conductivity versus composition plot, which is true of most of the composite systems studied so far. Since the $Na_2SO_4(Al_2O_3)$ system shows two conductivity peaks, we have met with limited success in our model-fitting endeavors.

Jow and Wagner (10) have proposed a qualitative model based on enhanced ionic conduction in the space charge layer around the alumina particles. They state that the enhanced conductivity, $\Delta\sigma$, is proportional to the surface area of added alumina, and is given by

$$\Delta\sigma \propto (1/r)[V_v/1 - V_v], \qquad [2]$$

where r and V_v are the radius and volume fraction of alumina particles, respectively. Figure 4 exhibits the observed variation in $\Delta\sigma$ with alumina volume fraction. It is evident that $\Delta\sigma$ is not proportional to the alumina volume fraction, as suggested by Jow and Wagner.

In their three-component resistor model, Roman *et al.* (21) emphasize the role of an enhanced interface conductivity. At two threshold concentrations, p'_c and p''_c, of the insulating phase, they predict critical properties corresponding to random conductor-semiconductor networks and normal conductor–insulator networks, respectively. They find the conductivity $\sum$ normalized by the value $\sum_o$ in the pure conductor to be related by

$$\sum(p)/\sum_o = (1 - p)[1 + \{(\tau - 1)/\tau\}\, 2^{d-1}\, p], \qquad [3]$$

where p is the mole fraction of the dispersed phase, τ is a model parameter given by $\tau = \sum_{max}/\sum_o$, for dimensionality $d = 3$. The $\sum(p)/\sum_o$ versus p graph is exhibited in Fig. 5.

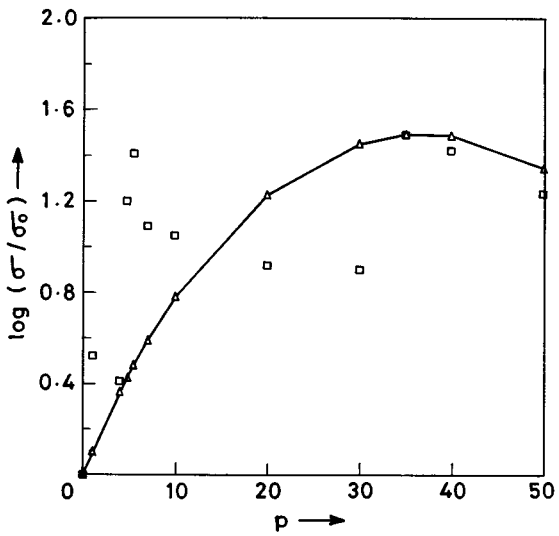

FIG. 5. Log (σ/σ_o) vs mole fraction of the dispersed phase (p). The experimental data (□) and the fitted curve for calculated values (△) using the model of Roman *et al.* are shown.

Again, the model of Roman *et al.* fails to explain the observed variation.

In an exhaustive review, Brailsford (23) has divided the electrical conductivity behavior of composite electrolytes into three major categories. In the composite systems showing Type I behavior, the conductivity decreases monotonously with increasing second-phase content. Type II behavior is characterized by an initial linear enhancement in conductivity on second-phase addition followed by smooth maximum, whereas Type III behavior corresponds to an initial insensitivity followed by a sharp, abrupt peak. While the former assumes that the conductivity enhancement is primarily due to the dispersoid-induced changes in the bulk conductivity of the matrix, the latter asserts that locally enhanced conduction is, in fact, the dominant factor. Our data seem to resemble a combination of Type II and Type III behavior as classified and later suggested by Brailsford. Type II behavior is given by

$$\sigma_M/\sigma_p = 2(1 - F)(1 + \eta F)/(2 + F), \qquad [4]$$

where σ_M and σ_p represent the conductivity of the composite and host, respectively, F is the alumina volume fraction, and η is a model parameter. Type III behavior is given by

$$\sigma_M(F)/\sigma_c = 4(1 - F)(1 - F')/(2 + F - 3F')(2 + F')$$
$$\text{for } F > F'. \qquad [5]$$

Here F' is some alumina volume fraction at which the conductivity is known, and σ_c is the same as σ_p.

Figure 6 shows a correlation of $\log(\sigma/\sigma_o)$ versus alumina volume fraction for these two mechanisms. For the Type II behavior, the value of model parameter η has been taken to be 100. It was calculated assuming that the conductivity enhancement is only due to Type II mechanism and not a combination of Type II and Type III mechanisms. For the Type III behavior, the conductivity value at 5.5 m/o Al_2O_3 has been used for calculations.

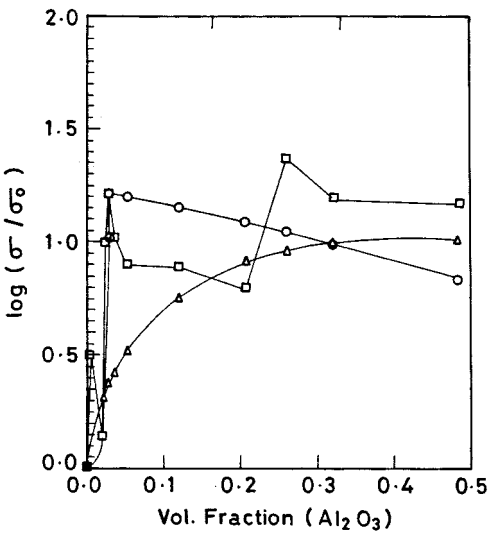

FIG. 6. Log (σ/σ_o) vs alumina volume fraction: (△) model Type II behavior; (○) model Type III behavior; (□) experimental data for 0.5 μm sized α-Al_2O_3 compositions.

Though the aforesaid behaviors represent two entirely different conductivity enhancement mechanisms, their combination is able to explain the conductivity versus composition behavior observed in the Na_2SO_4–Al_2O_3 system. It seems then, in our case, that the percolation mechanism dominates at smaller dispersoid volume fractions, and the sharp peak at 5.5 m/o Al_2O_3 indicates the establishment of percolation paths throughout the sample. As the alumina volume fraction was increased further, conductivity contributions from dispersoid-induced enhancements in the bulk conductivity become more significant, reaching a maximum at 35 m/o Al_2O_3 composition.

Any possible contribution from a highly conducting intermediate high-temperature phase is unlikely; DSC results rule out any thermal event that would otherwise accompany the observed changes in conductivity. However, a high-temperature XRD study would be required to substantiate this claim.

3.5. *Conductivity versus Form of Alumina*

Alumina occurs in many forms, among which γ-Al_2O_3 reportedly produces the maximum enhancement in conductivity in most systems (20). It is considered to be inert, and the effect is ascribed to a surface action, which leads to an increase in number of vacancies in the matrix material. This phenomenon, however, seems to be inoperative in the Na_2SO_4–Al_2O_3 system. The 5.5 and 35 m/o Al_2O_3 compositions show an enhancement by a factor of 20 with α-Al_2O_3 as the identified phase. Little or no enhancement is observed with γ-Al_2O_3 for these compositions. The log σ versus $10^3/T$ plots for Na_2SO_{4-x} m/o X-Al_2O_3 ($x = 4.75$, 5.5, 35, 40; $X = \alpha, \gamma$) are shown in Fig. 7. There has been one more instance in the literature (24) where γ-Al_2O_3 actually leads to a decrease in conductivity ($PbCl_2$–Al_2O_3). A more careful and detailed investigation of such systems along the lines of Shahi and Wagner (25) is required to obtain deeper insight into this selective enhancement phenomenon at the matrix–dispersoid interface.

3.6. *Conductivity versus Particle Size*

It is well known that the particle size of the dispersed phase plays a crucial role in the conductivity enhancement process. As the second-phase particle size decreases, the matrix–particle interface area increases. As a result, the volume fraction of the regions with locally enhanced

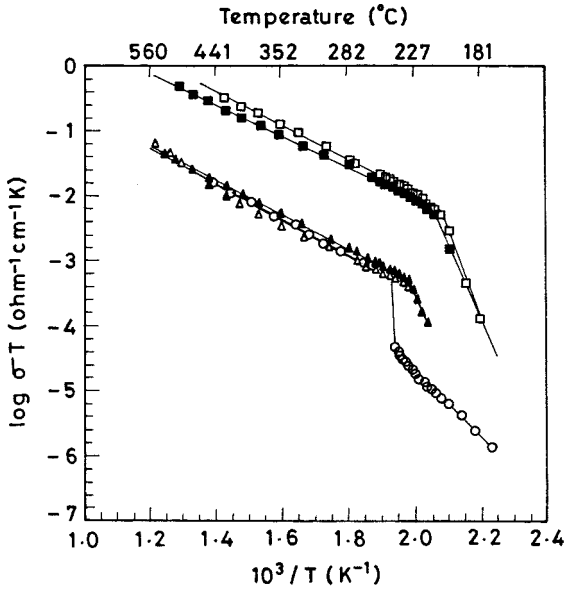

FIG. 7. Log σT vs form of alumina for x m/o Al_2O_3 (0.5 μm) compositions: pure Na_2SO_4 (○); $x = 5.5$, (□) α-Al_2O_3, (△) γ-Al_2O_3; $x = 35$, (■) α-Al_2O_3, (▲) γ-Al_2O_3.

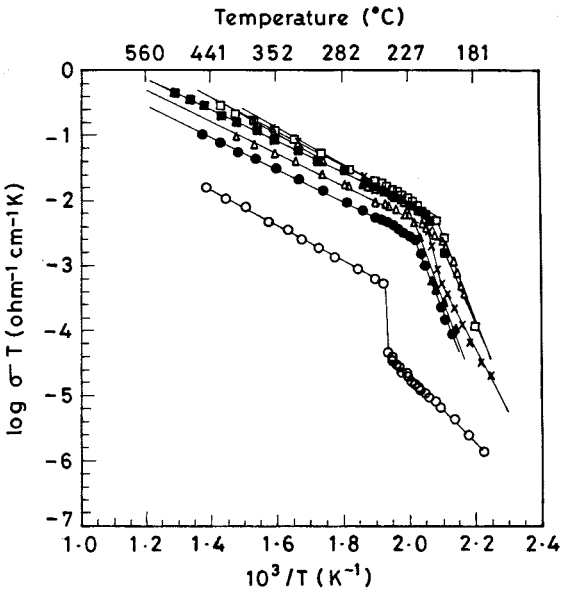

FIG. 8. Log σT vs particle size of alumina for x m/o α-Al_2O_3 compositions: pure Na_2SO_4 (○); $x = 4.75$, (△) 0.5 μm, (△) 0.004 μm; $x = 5.5$, (■) 0.5 μm, (×) 0.004 μm; $x = 35$, (□) 0.5 μm; (●) 0.004 μm.

conductivity increases dramatically, leading to an overall increase in conductivity.

Very little enhancement has been observed in composite electrolyte systems when the second-phase particle size was greater than 1 μm. In the Na_2SO_4–Al_2O_3 system, an enhancement by a factor of 20 was observed when Al_2O_3 of particle size 0.5 μm was used. Alumina of particle size 40 Å was also employed with an aim of further enhancing the conductivity. The log σT versus $10^3/T$ plots for 4.75, 5.5, and 35 m/o Al_2O_3 are shown in Fig. 8. No significant enhancement in conductivity for 40 Å alumina could be observed over 0.5 μm alumina. Even more interesting is the fact that for the 35 m/o composition, the dispersal of 40 Å Al_2O_3 results in a lower conductivity enhancement when compared to the 0.5 μm alumina. It is therefore appropriate to conclude that a tremendous increase in the surface area due to the 40 Å dispersed particles did not bring about a corresponding increase in the ionic conductivity.

The insensitivity of the particle size again contrasts with well-established composite theories that state an inverse relationship between conductivity and particle size. It indicates that although a certain minimum particle size (< 1 μm) is indeed required to obtain noticeable conductivity enhancement, the size factor perhaps becomes ineffective after some critical particle size. In his description of Type III behavior, Brailsford (23) has suggested a similar dependence on particle size as stated above. Dudney (26) has also pointed out that the reduction in particle size must be accompanied by an corresponding reduction in the matrix grain size if continuous increments in conductivity with decreasing particle size are to be obtained. The relationship between the second-phase particle size and matrix grain size, therefore, must be clearly understood if maximum enhancements in conductivity are to be engineered.

3.7. *Effect of Preparative Parameters*

It has been found that the conductivity enhancement process depends, to a large extent, on the preparative parameters (11). The various factors of importance are sample moisture content, heat-treatment temperatures, cooling rates, grain size, etc. As pointed out by several researchers, the conductivity enhancement process is quite sensitive to changes in the grain size. Zhu *et al.* (13) reported that in the Li_2SO_4–Al_2O_3 system, the highest conductivity is obtained when the grain size is the finest. The grain size, in turn, depends on the preparatory parameters.

To highlight the role of grain size, we chose the 4 m/o Al_2O_3 composition, which otherwise exhibits the least conductivity enhancement. The sample was heat treated at 1000°C. Instead of furnace cooling, it was quenched in air to obtain a finer-grained material.

The log σT versus $10^3/T$ plots for 4 m/o composition (furnace-cooled as well as the quenched samples) are shown in Fig. 9. Also shown are pure Na_2SO_4, and the 35 m/o Al_2O_3 furnace-cooled composition, which exhibits the maximum conductivity enhancement. Compared to the furnace-cooled 35 m/o Al_2O_3 composition, the 4 m/o quenched sample shows an increase in conductivity of 70 times for phase I. This enhancement is 2 orders of magnitude (105

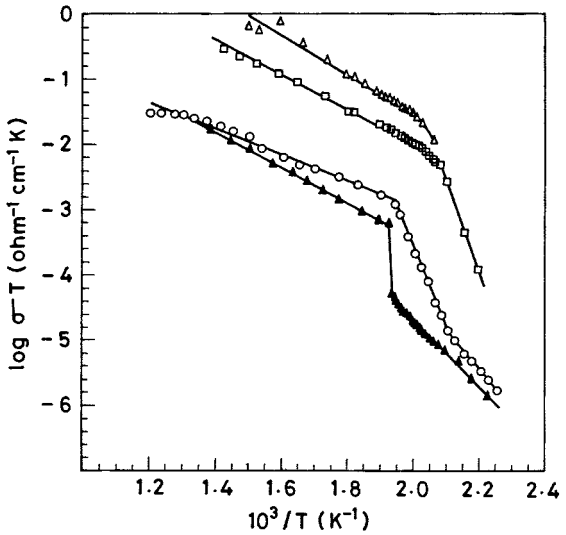

FIG. 9. Log σT vs $10^3/T$ for 4 m/o α-Al_2O_3 compositions, one furnace-cooled (○) and the other quenched (△). Also shown for comparison are pure Na_2SO_4 (▲) and the conductivity for the $x = 35$ (□) m/o Al_2O_3, which is the highest among furnace-cooled samples.

times) greater than that of Na_2SO_4-I at 400°C and over 3 orders of magnitude (1860 times) at 215°C. The increase in conductivity is also far greater than for the 35 m/o furnace-cooled composition, which shows enhancement by 20 times for phase I and 450 times at 200°C.

4. CONCLUSION

In this work, the influence of composition, particle size and form of alumina, and preparatory parameters on the electrical conductivity of Na_2SO_4 has been studied. The ionic conductivity of a wide range of compositions between 1 and 50 m/o Al_2O_3 of particle sizes 0.5 and 0.004 μm was measured. Two peaks were observed in conductivity versus composition plots at 5.5 and 35 m/o Al_2O_3, respectively. For the 35 m/o α-Al_2O_3, the conductivity increased around 20 times ($\sigma = 3.16 \times 10^{-4}$ ohm^{-1} cm^{-1}) at 400°C and 450 times ($\sigma = 5.6 \times 10^{-6}$ ohm^{-1} cm^{-1}) at 200°C.

It appears that two conductivity enhancement mechanisms, namely the percolation mechanism and the bulk mechanism, operate in the Na_2SO_4–Al_2O_3 system. The experimental data seem to resemble a combination of Type II and Type III behavior, as suggested by Brailsford (23). Reduction in the particle size of alumina from 0.5 to 0.004 μm does not bring about any further enhancement in conductivity. Also, negligible enhancements are observed when γ-Al_2O_3 is the identified phase. On the other hand, quenching leads to enhancements by 2 orders of magnitude at 400°C and more than 3 orders of magnitude at 200°C.

Presently, quenching studies of 5.5 and 35 m/o compositions are in progress. Attempts are underway to control the grain size of the matrix.

ACKNOWLEDGMENT

We are thankful to Dr. V. R. Palkar and Sumit Bhandari for providing us with 40 Å alumina.

REFERENCES

1. M. D. Leblanc, U. M. Gundusharma, and E. A. Secco, *Solid State Ionics* **20,** 16 (1986).
2. N. Rao and J. Schoonman, *Solid State Ionics* **57,** 159 (1992).
3. K. L.Keester, W. Eysel, and Th. Hahn, *Acta Crystallogr.* **A31,** S79 (1975).
4. A. Singhvi, S. Gomathy, P. Gopalan, and A. R. Kulkarni, *J. Solid State Chem.* **138,** 183 (1998).
5. H. H. Hofer, W. Eysel, and U. Von Alpen, *Mater. Res. Bull.* **13,** 135 (1978).
6. K. Shahi and G. Prakash, *Solid State Ionics* **18/19,** 544 (1987).
7. G. Prakash and K. Shahi, *Solid State Ionics* **23,** 151 (1987).
8. P. Chowdhary, V. B. Tare, and J. B. Wagner, Jr., *J. Electrochem. Soc.* **132,** 123 (1985).
9. J. B. Wagner, Jr., *Mater. Res. Bull.* **15,** 1691 (1980).
10. T. Jow and J.B. Wagner, Jr, *J. Electrochem. Soc.* **126,** 1973 (1979).
11. N. J. Dudney, *Annu. Rev. Mater. Sci.* **19,** 103 (1989).
12. J. Maier, *Phys. Stat. Sol.* (*b*) **123,** K89 (1984).
13. J. Maier, *Ber. Bunsenges. Phys. Chem.* **88,** 1057 (1984).
14. J. Maier, *J. Phys. Chem. Solids* **46,** 309 (1985).
15. J. Maier, *J. Electrochem. Soc.* **134,** 1524 (1987).
16. J. Maier, *Prog. Solid State Chem.* **23,** 171 (1995).
17. J. Maier, *Solid State Ionics* **75,** 139 (1995).
18. J. Maier, *J. Eur. Ceram. Soc.* **19,** 675 (1999).
19. C. C. Liang, *J. Electrochem. Soc.* **120,** 1289 (1973).
20. B. Zhu, Z. H. Lai, and B. E. Mellander, *Solid State Ionics* **70/71,** 125 (1994).
21. H. E. Roman, A. Bunde, and W. Dietrich, *Phys. Rev.* **B34,** 3479 (1986).
22. C. Wagner, *J. Phys. Chem. Solids* **33,** 1051 (1972).
23. A. D. Brailsford, *Solid State Ionics* **21,** 159 (1986).
24. A. Bunde and J. B. Wagner, Jr., *Solid State Ionics* **25,** 165 (1987).
25. K. Shahi and J. B. Wagner, Jr., *J. Solid State Chem.* **42,** 107 (1982).
26. N. J. Dudney, *J. Am Ceram. Soc.* **68,** 538 (1985).